Arch. Metall. Mater. **64** (2019), 3, 1011-1016

DOI: 10.24425/amm.2019.129488

M. KAROLUS*#, J. MASZYBROCKA*, A. STWORA**, G. SKRABALAK**

RESIDUAL STRESSES OF AlSi10Mg FABRICATED BY SELECTIVE LASER MELTING (SLM)

The aim of the paper is the residual stress analysis of AlSi10Mg material fabricated by selective laser melting (SLM). The SLM technique allows to product of complex geometries based on three-dimensional model, in which stiffness and porosity can be precisely designed for specific uses. As the studied material, there were chosen solid samples built in two different directions: parallel (P-L) and perpendicular (P-R) to the tested surface and cellular lattice built in perpendicular direction, as well. In the paper, for the complex characterization of obtained materials, the phase analysis, residual stress and texture studies were performed. The classical non-destructive $\sin^2\psi$ method was used to measure the residual stress measurements.

The final products, both solid sample and cellular lattice, have a homogeneous phase composition and consist of solid solution Al(Si) (Fm-3m) type, Si (Fd-3m) and Mg_2Si (Pnma). The obtained values of the crystallite size are in a range of 1000 Å for Al(Si), 130-180 Å for Si phase. For Mg_2Si phase, the crystallite sizes depend on sintering process, they are 800 Å for solid samples and 107 Å for cellular lattice. The residual stress results have the compressive character and they are in a range from –5 to –15 MPa.

Keywords: AlSi10Mg alloys, Selective Laser Melting (SLM), XRD, residual stress – $\sin^2\psi$ method, texture

1. Introduction

Selective Laser Melting (SLM) technology is currently one of the most dynamically developing incremental / additive manufacturing method [1,2]. Along with technological progress, a significant increase in the share of this segment in the entire market production is observed. Selective Laser Melting process is an incremental method developed in the 1980s. Nowadays, Selective Laser Sintering and Selective Laser Melting (SLS/SLM) are one of the fastest growing branches associated with additive manufacturing technologies. Unlimited possibilities as to the shape of the elements being made and the ability to create internal channels with complex geometry, make the SLS/SLM technologies applicable, among others, in the tool industry (making injection molds equipped with conformal cooling channels), in the medical industry (making parts hip and knee joint implants), in the aerospace industry (making turbine blades and fuel injectors for aircraft engines) [3-6].

Presented in the paper material – AlSi10Mg is a typical casting alloy, often used for pressure casting. Its good mechanical properties combined with light weight and flexible post-processing capabilities have made it a widely used material in the automotive and aerospace industries [7]. Despite the passage of years, there has been a steady increase in the demand for aluminum components. This is connected, among others, with the development of new vehicle concepts and the search for opportunities to reduce their weight [8]. The use of SLM technology opens up new possibilities in this field. In particular, this applies to components with complex geometry, including components with a cellular structure (cellular lattice) [9,10]. Discussed alloy is relatively young material for SLM technique, comparing to 316L steel or titanium alloys Ti6Al4V. First successful, practical applications of AlSi10Mg in SLM was dated around 2010. Since then, numerous researches have been carried out towards verification of laser melted AlSi10Mg in comparison with casted components [11-14]. To maximize the potential of the SLM process for the AlSi10Mg alloy, the majority of research is focused on the optimization of process parameters (i.e. energy density, scanning strategy, hatch space), which aims to obtain high quality products [15-17]. This is a complicated task, because the high thermal conductivity of aluminum-based powders and a reflectivity make necessary the use of a high laser power for melting and to overcome the rapid heat dissipation. Moreover the aluminum powder shows low flowability (a good powder flowability is required to achieve constant thickness powder layers). The influence of SLM process parameters is widely described in the literature with reference to the density, surface topology, and dimensional accuracy of AlSi10Mg, microstructure or mechanical properties obtained [18,19]. Results of research conducted by Kempen et al. [16] show that AlSi10Mg parts created with SLM process have good mechanical properties, comparable or even better than parts manufactured with casting processes.

* UNIVERSITY OF SILESIA, INSTITUTE OF MATERIALS SCIENCE, 1 A 75 PUŁKU PIECHOTY STR., 41-500 CHORZÓW, POLAND
** INSTITUTE OF ADVANCED MANUFACTURING TECHNOLOGY, 37A WROCŁAWSKA STR., 30-011 KRAKÓW, POLAND

Corresponding author: karolus@us.edu.pl

To ensure the required quality of selectively melted elements from the AlSi10Mg alloy, it is also necessary, in addition to optimizing the melting parameters [20-22], to select the direction of the model's production. Research Kempen et al. [16] showed that AlSi10Mg samples produced by SLM at different angles show the anisotropy of mechanical properties. The reason for this might be a larger borderline porosity, which makes the Z-oriented tensile parts are more sensitive to crack initiation, compared to XY oriented tensile samples.

Part of the research focuses on determining residual stresses in melted layers that are created because of the high temperature gradients, thermal expansion and non-uniform plastic deformation during heating and cooling cycle [23,24]. Studding the literature there is possible to notice that the distribution of residual stresses in materials obtained by SLM technique is depended on material chemical composition, temperature treatment, sintering parameters and direction [25-29].

In the literature, one can find works on the analysis of the distribution of internal stresses in materials obtained by SLM technique. For example, in [26,28] works there are presented results of residual stress measurements obtained for AlSi10Mg alloy by use of semi-destructive hole-drilling method. An important aspect of that method is the fact that such experiment needs specialized equipment and destroys material. In that work, the authors would like to present the use of the standard X-ray diffractometer and the classical non-destructive $\sin^2\psi$ method, allowing a relatively simple determination of the character of residual stresses in the material.

The aim of this work is the structural characterization of AlSi10Mg material fabricated by SLM technique and evaluation the effect of the orientation of the element being built on the residual stresses and texture.

2. Material

The tested AlSi10Mg material were manufactured from Renishaw AlSi10Mg powders. The chemical composition of the initial AlSi10Mg powder is shown in Table 1.

As the studied material, powder with a mean grain size of 50 μm was used. SEM images have shown differences in shape and particle size (30÷50 μm in diameter – Fig. 1a), as well. Such material is not preferable for the SLM technique, as it might significantly affect the homogeneity and porosity of the obtained structure. The SEM images of the final cellular lattice are shown on the Fig. 1b.

For testing, there were chosen solid samples sintered in two different directions: perpendicular (P-R) and parallel (P-L) to the tested surface and cellular lattice sample sintered in perpendicular direction (C-L) (Fig. 2-4).

3. Experimental

3.1. Selective Laser Melting (SLM)

In order to avoid melting elements with numerous inhomogeneities and failure of the building process, appropriate melting parameters should be selected. So, the samples were obtained using a selective laser melting device AM 250 Renishaw equipped with a fiber laser Yb-Fiber (λ = 1064 nm) with a power of 400 W in Institute of Advanced Manufacturing Technology (Cracow, Poland). During the process, inert gas atmosphere (oxygen content below 100 ppm) was used in the working chamber. Melting parameters are presented in Table 2. Technological parameters and model preparation for the SLM process were performed in Autofab software.

TABLE 1

Chemical composition of AlSi10Mg powder

Element	Al	Si	Mg	Fe	N	O	Ti	Zn	Mn	Ni	Cu	Pb	Sn
wt.%	balance	9.00-11.00	0.25-0.45	<0.25	<0.20	<0.20	<0.15	<0.10	<0.10	<0.05	<0.05	<0.02	<0.02

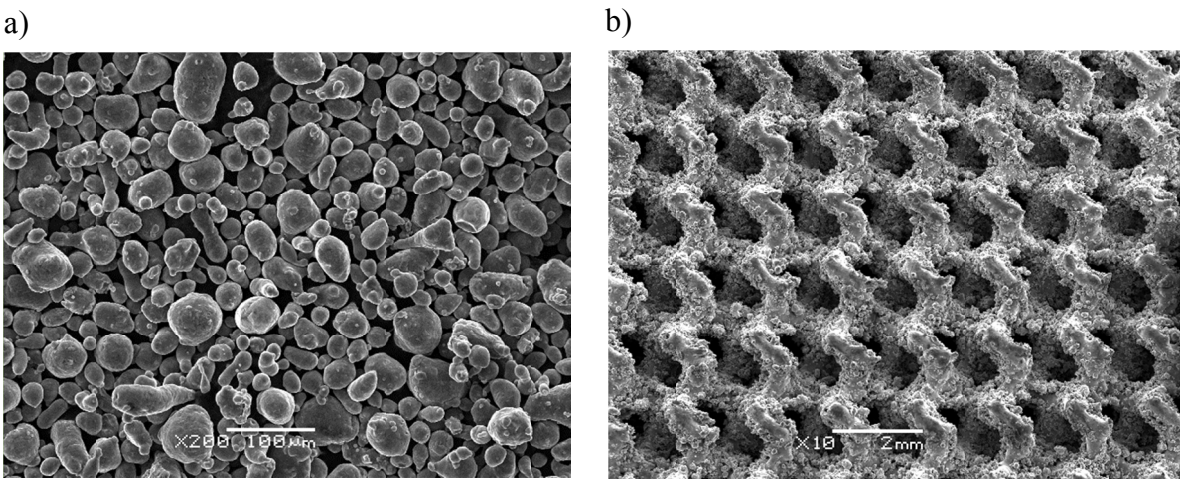

Fig. 1. SEM images of: a) initial AlSi10Mg powder and b) final cellular lattice

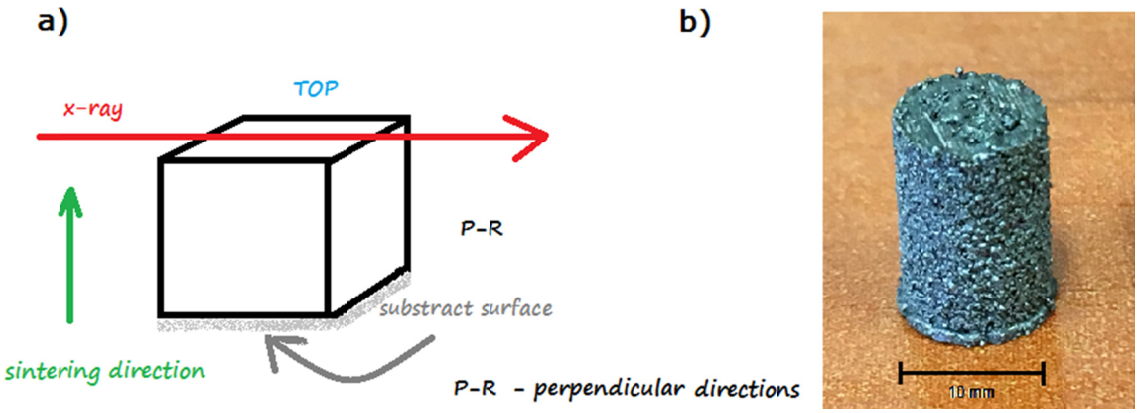

Fig. 2. Scheme of the sample orientation: a) during the SLM process and the XRD experiments and b) solid sample after SLM process – perpendicular (P-R)

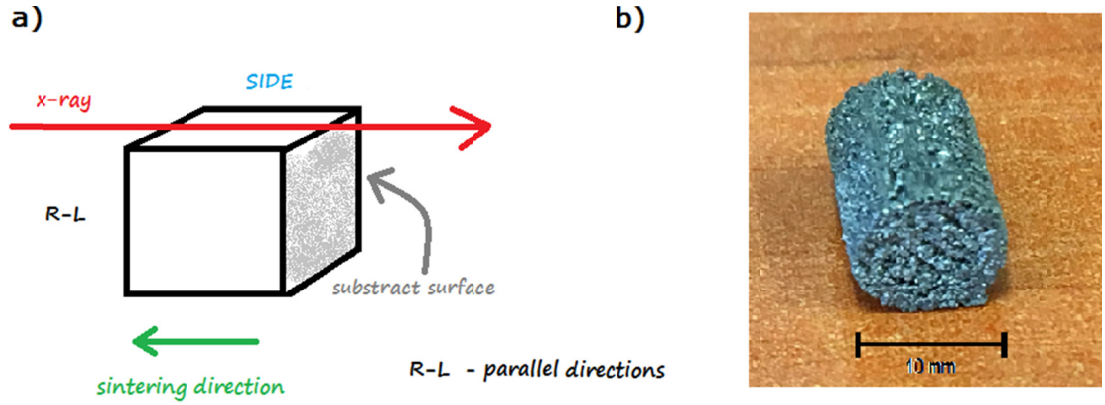

Fig. 3. Scheme of the sample orientation: a) during the SLM process and the XRD experiments and b) solid sample after SLM process – parallel (P-L)

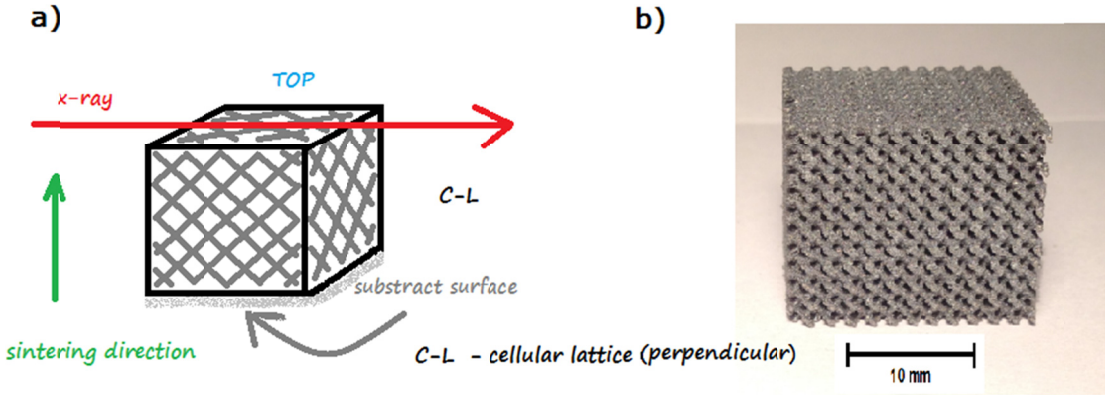

Fig. 4. Scheme of the sample orientation: a) during the SLM process and the XRD experiments and b) cellular lattice sample after SLM process – perpendicular direction (C-L)

TABLE 2

Parameters of SLM technology during sintering of ALSI10Mg samples

Parameters	Values
Layer thickness	50 [µm]
Point Distance	75 [µm]
Exposure Time	75 [µs]
Laser Power	400 [W]
Scan Speed	150 [mm/s]
The angle of inclination of the samples	0 [°] (P-R) and 90 [°] (P-L)

The orientation of the samples during the building process were shown on Fig. 2-4. After finishing of the process, the samples were cut off from the base plate, using electrical discharge machining (EDM) wire cutting.

3.2. XRD analysis

The XRD measurements were performed using the X-ray diffractometer Empyrean PANalytical equipped with the

5-axis stage, cobalt radiation (Co Kα_1 = 1.79021 Å), PIXcel and scintillation detectors. The HighScore Plus software and ICDD data base (PDF4+ 2016) were used for phase identification. Structure refinements, unit cell parameters, crystallite sizes and lattice strains of identified phases were analyzed by the Rietveld refinement basing on the Williamson-Hall theory [30-32]. The calculation of the crystallite size and lattice strain was based on the whole angle X-ray scattering (WAXS) pattern analysis [33]. Residual stress [34] analysis was performed for all tested samples for Al (311) diffraction line. Texture analysis was performed for Al (200) diffraction plane. The calculations were carried out with the PANalytical software X'Pert Stress and X'Pert Texture, respectively.

4. Results and discussion

The final products, both solid sample and cellular lattice, have a homogeneous phase composition and consist of solid solution Al(Si) (Fm-3m) type, Si (Fd-3m) and Mg_2Si (Pnma) phases in an amount range of 92-94, 4-7 and 1-3 wt.%. The example of X-ray diffraction patterns obtained for solid and cellular lattice are presented on Fig. 5.

The results of unit cell refinement and structural characterization parameters are presented in Table 3-5. The slight changes in values of Al unit cell parameters in comparison to the theoretical ones (ICDD PDF4+ 2016 card: 00-004-0787; a = 4.0494 Å) indicate the formation of the solid solution Al(Si) type.

The aluminum crystallite size analysis gives similar results for all samples – in a range of 1000 Å for Al(Si) and 130-180 Å for Si phase. However, the differences in the crystallite sizes of Mg_2Si phase in dependence on sintering process were observed (800 Å for solid samples and 107 Å for cellular lattice).

In the solid sample (P-R - tested surface perpendicular to the building direction), the texture of aluminum phase of (200) diffraction plane was observed. The example of pole figures are presented on Fig. 6.

TABLE 3

The structural results of AlSi10Mg solid sample, P-R (perpendicular)

Phase	ICDD PDF4+	Unit cell parameters: a/c [Å]	Space Group	Phase amount [wt.%]	Crystallite size: D [Å]
Al	98-018-2727	4.0512(1)	F m-3m	94	>1000
Si	04-007-8736	5.4310(1)/ 6.5952(4)	F d-3m	4	180
Mg_2Si	98-016-7511	3.9820(5)/ 7.7236(5)	P nma	2	800

TABLE 4

The structural results of AlSi10Mg solid sample, P-L (parallel)

Phase	ICDD PDF4+	Unit cell parameters: a/c [Å]	Space Group	Phase amount [wt.%]	Crystallite size: D [Å]
Al	98-018-2727	4.0550(6))	F m-3m	92	950
Si	04-007-8736	5.4381(5)/ 6.5993(1)	F d-3m	7	115
Mg_2Si	98-016-7511	3.9909(6)/ 7.7833(8)	P nma	1	760

TABLE 5

The structural analysis results of AlSi10Mg cellular lattice, C-L (perpendicular)

Phase	ICDD PDF4+	Unit cell parameters: a/c [Å]	Space Group	Phase amount [wt.%]	Crystallite size: D [Å]
Al	00-004-0787	4.0481(1)	F m-3m	92	> 1000
Si	04-007-8736	5.4275(9)/ 6.5797(8)	F d-3m	5	130
Mg_2Si	98-016-7511	3.9381(9)/ 7.7378(2)	P nma	3	107

The residual stress analysis performed for Al (311) diffraction line indicates their compressive character. The detailed results are presented on Fig. 7 and Tables 6 and 7.

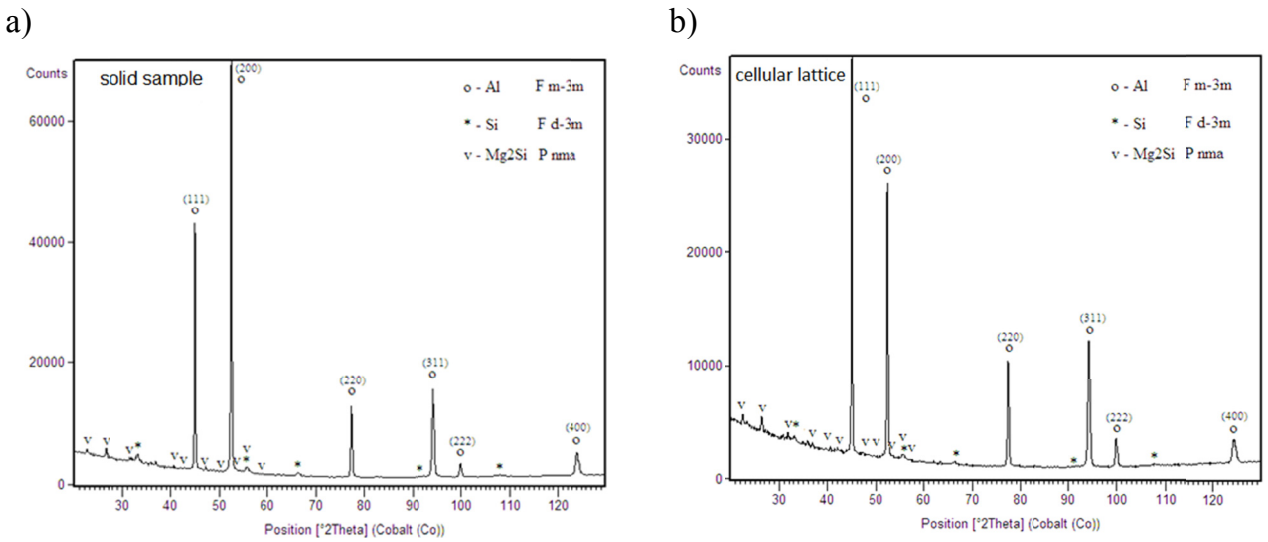

Fig. 5. The examples of X-ray diffraction patterns obtained for a) solid and b) cellular lattice of AlSi10Mg samples (perpendicular direction)

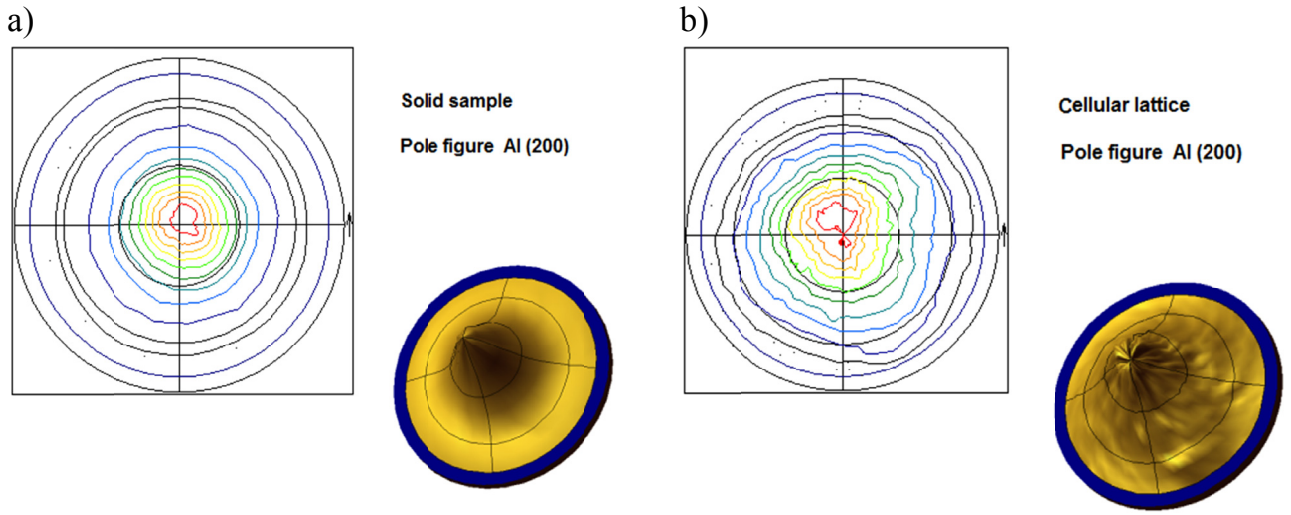

Fig. 6. The examples of pole figures obtained for a) solid (perpendicular direction) and b) cellular lattice of AlSi10Mg samples

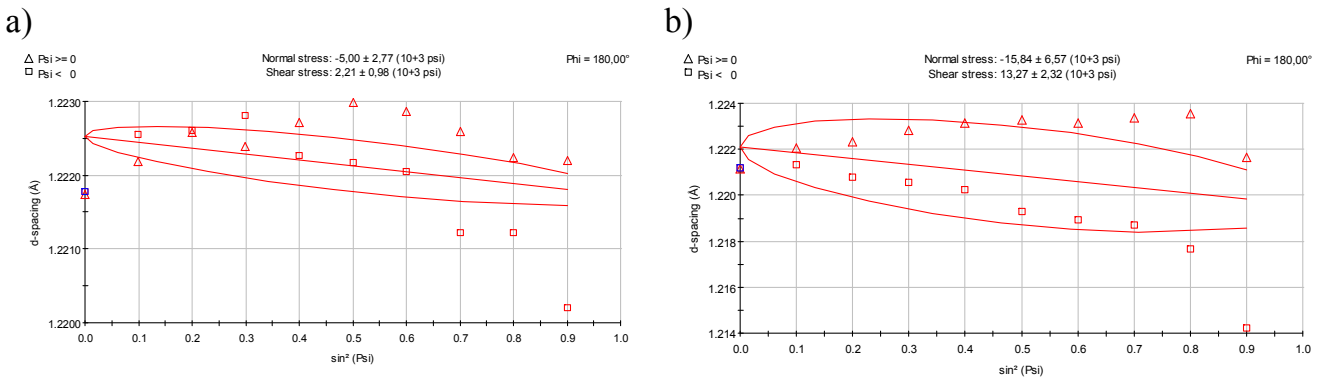

Fig. 7. The examples of residual stress diagrams obtained for a) solid and b) cellular lattice of AlSi10Mg samples (perpendicular direction)

TABLE 6

Residual stress results of AlSi10Mg obtained for solid sample, P-R (perpendicular direction)

	ϕ:	0°	45°	90°	135°
Al (311)	σ **[MPa]**	–5.00	–4.76	–0.75	–2.56

TABLE 7

Residual stress results of AlSi10Mg obtained for cellular lattice, C-L (perpendicular direction)

	ϕ:	0°	45°	90°	135°
Al (311)	σ **[MPa]**	–15.84	–23.39	–19.52	–16.28

The obtained residual stresses results reached values of about –5 MPa for the solid sample and –15 MPa for the cellular lattice. Not linear character of residual stress diagrams (especially observed for solid sample – Fig. 7a) indicates nonhomogenity of material. In comparison to other results known from literature [26,28], one can observed that residual stresses for AlSi10Mg alloys measured by use of semi-destructive hole-drilling method were on level of 55-66 MPa. The visible difference in obtained values might be an effect of influence of direct contact between the sample and the support plate and thus generating stresses [28].

5. Conclusions

In general, it can be concluded that the direction of process, increase in density, decrease in porosity affect the structural changes, e.g. occurrence and distribution of texture and presence of residual stresses in the material. All tested samples are characterized by compressive residual stresses. Moreover, the residual stresses character and values obtained for cellular lattice are more stable then residual stress obtained for solid samples. The results have pointed out that:

– the final products, both solid sample and cellular lattice, have a homogeneous phase composition and consist of solid solution Al(Si) (Fm-3m) type, Si (Fd-3m) and Mg_2Si (Pnma);
– the obtained crystallite size in studied AlSi10Mg material are in a range of 1000 Å for Al(Si), 130-180 Å for Si phase;
– for Mg_2Si phase, the crystallite sizes depend on building process, they are 800 Å for solid samples and 107 Å for cellular lattice;
– the residual stress results have the compressive character and they are on the level from –5 to –15 MPa.

REFERENCES

[1] T. Wohlers, T. Caffrey, Wohler's report 2018 – 3D Printing and Additive Manufacturing State of the Industry, Annual Worldwide Progress Report (2018).

[2] S. Bremen, W. Meiners, A. Diatlov, Laser Tech. J. (2012), DOI: 10.1002/latj.201290018.

[3] J. Banhart, Int. J. Veh. Des. (2005), DOI: 10.1504/ijvd.2005.006640.

[4] E.O. Olakanmi, R.F. Cochrane, K.W. Dalgarno, Prog. Mater. Sci. (2015), DOI: 10.1016/j.pmatsci.2015.03.002.

[5] J. Pakkanen, F. Calignano, F. Trevisan, M. Lorusso, E.P. Ambrosio, D. Manfredi, P. Fino, Metall. Mater. Trans. A Phys. Metall. Mater. Sci. (2016), DOI: 10.1007/s11661-016-3478-7.

[6] A. Armillotta, R. Baraggi, S. Fasoli, Int. J. Adv. Manuf. Technol. (2014), DOI: 10.1007/s00170-013-5523-7.

[7] R.P. Bajpai, U. Chandrasekhar, A. Arankalle, in: Int. Conf. Innov. Des. Anal. Dev. Pract. Aerosp. Automot. Eng. (IDAD 2014) DOI: 10.1007/978-81-322-1871-5.

[8] M. Tisza, I. Czinege, Int. J. Light. Mater. Manuf. (2018), DOI: 10.1016/j.ijlmm.2018.09.001.

[9] C. Yan, L. Hao, A. Hussein, S.L. Bubb, P. Young, D. Raymont, J. Mater. Process. Technol. (2014), DOI: 10.1016/j.jmatprotec.2013.12.004.

[10] X. Han, H. Zhu, X. Nie, G. Wang, X. Zeng, Materials (Basel) (2018), DOI: 10.3390/ma11030392.

[11] K. Kempen, L. Thijs, J. Van Humbeeck, J.P. Kruth, in: Phys. Procedia (2012), DOI: 10.1016/j.phpro.2012.10.059.

[12] C.A. Biffi, J. Fiocchi, P. Bassani, D.S. Paolino, A. Tridello, G. Chiandussi, M. Rossetto, A. Tuissi, Procedia Struct. Integr. (2017), DOI: 10.1016/J.PROSTR.2017.11.060.

[13] K. Bartkowiak, S. Ullrich, T. Frick, M. Schmidt, in: Phys. Procedia (2011), DOI: 10.1016/j.phpro.2011.03.050.

[14] D. Buchbinder, H. Schleifenbaum, S. Heidrich, W. Meiners, J. Bültmann, in: Phys. Procedia (2011), DOI: 10.1016/j.phpro.2011.03.035.

[15] Y. Liu, C. Liu, W. Liu, Y. Ma, S. Tang, C. Liang, Q. Cai, C. Zhang, Opt. Laser Technol. (2019), DOI: 10.1016/j.optlastec.2018.10.030.

[16] K. Kempen, L. Thijs, E. Yasa, M. Badrossamay, W. Verheecke, J.P. Kruth, in: Proc. 22nd Solid Free. Fabr. Symp. (2011).

[17] B.A.I. Shigang, N. Perevoshchikova, Y. Sha, X. Wu, Applied Sciences. (2019), DOI: 10.3390/app9030583.

[18] A.H. Maamoun, Y.F. Xue, M.A. Elbestawi, S.C. Veldhuis, Materials (Basel) (2018), doi:10.3390/ma11122343.

[19] F. Trevisan, F. Calignano, M. Lorusso, J. Pakkanen, A. Aversa, E.P. Ambrosio, M. Lombardi, P. Fino, D. Manfredi, Materials (Basel) (2017), DOI: 10.3390/ma10010076.

[20] N.T. Aboulkhair, N.M. Everitt, I. Ashcroft, C. Tuck, Addit. Manuf. (2014), DOI: 10.1016/j.addma.2014.08.001.

[21] M. Krishnan, E. Atzeni, R. Canali, F. Calignano, D.E. Manfredi, P. Ambrosio, L. Iuliano, Rapid Prototyp. J. (2014), DOI: 10.1108/RPJ-03-2013-0028.

[22] Z. Chen, Z. Wei, P. Wei, S. Chen, B. Lu, J. Du, J. Li, S. Zhang, J. Mater. Eng. Perform. (2017), DOI: 10.1007/s11665-017-3044-5.

[23] C. López, A. Elías-Zúñiga, I. Jiménez, O. Martínez-Romero, H.R. Siller, J.M. Diabb, Materials (Basel) (2018), DOI: 10.3390/ma11122542.

[24] J. Wu, L. Wang, X. An, Optik (Stuttg) (2017), DOI: 10.1016/j.ijleo.2017.02.060.

[25] L. Wang, X. Jiang, Y. Zhu, Z. Ding, X. Zhu, J. Sun, B. Yan, Adv. Mater. Sci. Eng. (2018), DOI: 10.1155/2018/7814039.

[26] A. Salmi, E. Atzeni, Virtual Phys. Prototyp. (2017), DOI: 10.1080/17452759.2017.1310439.

[27] B. Vrancken, R. Wauthle, J. Kruth, J. Van Humbeeck, Proc. 24th Int. Solid Free. Fabr. Symp. (2013), DOI: 10.1016/j.neuropsychologia.2011.03.040.

[28] A. Salmi, E. Atzeni, L. Iuliano, M. Galati, In Proceedings of the Procedia CIRP (2017), DOI: 10.1016/j.procir.2016.06.030.

[29] L. Wang, X. Jiang, Y. Zhu, Z. Ding, X. Zhu, J. Sun, B. Yan, Adv. Mater. Sci. Eng. (2018), DOI: 10.1007/s00170-018-2207-3.

[30] R. Young, The Rietveld Method. Int. Union Crystallogr. B. Ser. 1993.

[31] L.B. Mc Cusker, R.B. Von Dreele, D.E. Cox, D. Louër, P. Scardi, J. Appl. Cryst. **32**, 36-50 (1999), DOI: 10.1107/S0021889898009856.

[32] G.K. Williamson, W.H. Hall, Acta Metall. (1953), DOI: 10.1016/0001-6160(53)90006-6.

[33] M. Karolus, E. Łągiewka, J. Alloys Compd. **367**, 235-238 (2004), DOI: 10.1016/j.jallcom.2003.08.044.

[34] N.W. Gregory, Elements of X-Ray Diffraction. J. Am. Chem. Soc. (1957), DOI: 10.1021/ja01564a077.